Electrodeposition of Vertically Aligned Palladium Nanoneedles and Their Application as Active Substrates for Surface-Enhanced Raman Scattering

ARTICLE *in* THE JOURNAL OF PHYSICAL CHEMISTRY C · APRIL 2014

Impact Factor: 4.77 · DOI: 10.1021/jp500667f

4 AUTHORS, INCLUDING:

Peng Diao
Beihang University(BUAA)
78 PUBLICATIONS **1,795** CITATIONS

SEE PROFILE

THE JOURNAL OF PHYSICAL CHEMISTRY C

Article

pubs.acs.org/JPCC

Electrodeposition of Vertically Aligned Palladium Nanoneedles and Their Application as Active Substrates for Surface-Enhanced Raman Scattering

Di Xu,[†] Xiaohui Yan,[†] Peng Diao,*[,†] and Penggang Yin[‡]

[†]School of Materials Science and Engineering, Beihang University, Beijing 100191, P. R. China

[‡]School of Chemistry and Environment, Beihang University, Beijing 100191, P. R. China

Supporting Information

ABSTRACT: Vertically aligned Pd nanoneedles (NNs) with high aspect ratio and uniform growth density were fabricated on indium tin oxide (ITO) substrates by a facile electrodeposition method, which consisted of a short nanoseed-generating step followed by a growth step. The obtained Pd NNs have a full width at half-maximum (fwhm) of 22 ± 8 nm and taper angle of 15 ± 4°. X-ray diffraction (XRD) and high-resolution transmission electron microscopic (HRTEM) results imply that the NNs were built through the stacking of {111} facets. The factors influencing the electrochemical nucleation and growth of Pd NNs were systematically studied. It was found that the transient nucleation step at a highly negative overpotential is prerequisite to the formation of the uniformly dispersed and vertically aligned Pd NNs. The morphology, size, and aspect ratio of Pd nanocrystals (NCs) were extremely sensitive to the potential applied in the growth step. High aspect ratio and well-aligned Pd NNs could only be obtained in a narrow potential range from 0.100 to 0.200 V. Bromide ions played a dominant role in shaping the morphology of Pd NCs, while citrate ions acted as an assistant shape-controlling agent. A concentration-gradient-induced growth mechanism of Pd NNs was proposed on the basis of the time-dependent scanning electron microscopic (SEM) results. The formation of a uniform diffusion layer at the Pd NNs/solution interface and the concentration gradient of the precursor within the diffusion layer were responsible for the vertically oriented growth of Pd NNs. The Pd NNs exhibited good surface-enhanced Raman scattering (SERS) activity under the excitation of 488 nm laser, implying its potential application as a SERS substrate. The SERS activity of Pd NNs was attributed to the unique morphology and the perpendicular alignment of Pd NNs.

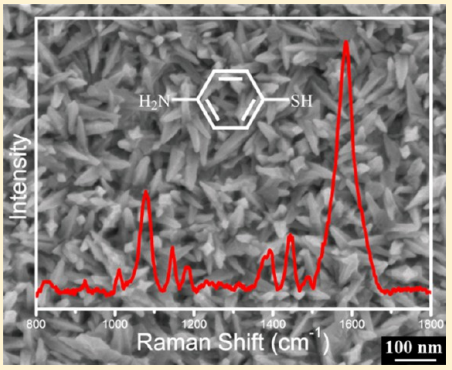

1. INTRODUCTION

As a member of the noble metal family, Pd has attracted extensive attention over the past decades because of its promising applications in numerous fields such as catalysis,[1,2] sensing,[3] and SERS.[4] However, the high cost of Pd prevents its application in many areas at a large industrial scale. The preparation of Pd particles with high mass activity (activity per unit mass) provides a feasible solution. There are two main ways to improve the mass activity of a crystalline catalyst. One is to increase the specific area of the catalyst, and the other is to expose the highly active facets. For the first way, one can enlarge the specific area by simply decreasing the size of catalyst particles, i.e., synthesizing nanocrystals (NCs). For the second way, however, it is not easy to control the exposed facets of the crystalline catalysts. Therefore, synthesizing noble nanoparticles with desired exposed facets received a great deal of attention in recent years due to its difficulties and potential application in many fields.[5,6] It is desirable to combine the above two strategies together in one approach, that is, to synthesize noble metal NCs while controlling both the size and the morphology.[7] Solution synthesis by introducing capping agents into reaction system has been proved to be successful in size- and morphology-controlled synthesis of noble metal NCs, such as Au,[8,9] Pt,[10,11] Ag,[12,13] and Rh.[14,15] Great effort has also been focused on the shape-controlled synthesis of Pd NCs in solution, and diverse Pd nanostructures including nanorods,[1] nanowires,[16] nanocubes,[17,18] nanodendrites,[1,18] nanoplates,[19] and nanopolyhedrons[20,21] have been successfully prepared.

The noble metal NCs synthesized in solution have to be dispersed on solid substrate for many applications, such as catalysis,[22,23] electrocatalysis,[6,24,25] and sensing.[26−28] Therefore, direct surface growth of noble metal NCs on substrates is highly desirable. However, morphology- and size-controlled growth of noble metal NCs on solid substrate is more difficult than solution synthesis due to the complexity of the heterogeneous interface. Moreover, it should be pointed out here that the purification methods such as centrifugation,[8−11,13−19] filtration,[12] and electrophoresis,[29] which were

Received: January 20, 2014
Revised: April 8, 2014
Published: April 21, 2014

   dx.doi.org/10.1021/jp500667f | J. Phys. Chem. C 2014, 118, 9758−9768

widely used in solution synthesis to enrich the NCs with the same morphology and size, cannot be used in the direct surface growth. In other words, the yield of certain NCs in electrodeposition reflects the real yield in the synthesis process. This further increases the difficulty in preparing NCs with desired size and morphology.

Electrochemical deposition is a convenient approach to preparing metal NCs on conducting substrates.[7] As one of the surface growth approaches, electrodeposition also faces the above-mentioned challenges in growing NCs with desired size and morphology. Despite the challenges, many effects have been made to prepare noble metal NCs on conductive substrates by electrochemical methods because of the following three reasons: (1) The growth rate of NCs can be conveniently controlled by the applied potential because the potential dominates the reduction rate of precursors. (2) The adsorption and desorption behaviors of capping agent on different facets of NCs can be monitored by tuning the applied potential, making it possible for some facets to be blocked by the capping agents while leaving others still accessible to the precursors. (3) The presence of concentration gradient of the precursor at electrode/solution interface may influence the growth orientation of NCs. There are several reports concerning shape-controlled electrochemical synthesis of noble metal NCs, such as Pt,[30,31] Au,[32,33] Rh,[34] and Ag[35] as well.

Electrochemical methods were also employed for morphology-controlled synthesis of Pd NCs.[36−39] Tian and co-workers adopted a square-wave potential method to prepare Pd NCs on glassy carbon electrodes. The obtained Pd NCs were enclosed by high-index facets, which was responsible for their high electrocatalytic activity.[36] Jia et al. reported the deposition of Pd nanoplate and nanotree arrays by using a template-free cyclic potential sweep approach. The resulting Pd nanostructures exhibited high electrocatalytic activity toward ethanol oxidation.[37] Fang et al. reported the electrodeposition of Pd nanourchins that showed high activity toward formic acid electrooxidation.[38] Moreover, Pd dendritic nanowires were also synthesized by electrodeposition.[39]

Besides catalytic properties, surface-enhanced Raman scattering (SERS) activity of Pd was also confirmed by previous work,[19] revealing the potential application of Pd nanostructures as SERS active substrates. The chemical enhancement and the electromagnetic enhancement are two widely accepted mechanisms for SERS. The chemical enhancement is closely related to the compositions of both the surface structure and the adsorbed molecules, while the electromagnetic enhancement is dependent on the size, morphology, and orientation of the nanostructures. The shape and the orientation of metal NCs are important factors that determine their SERS properties, especially when the anisotropic NCs are parallelly or vertically aligned on substrates.[40] From the viewpoint of electromagnetic enhancement, the vertically aligned nanorods (or nanoneedles) with pointed top ends are highly desirable because the sharp ends can greatly enhance the local field and the vertical alignment may intensify the interaction of incident light with nanorods (or nanoneedles).

In this work, we report the preparation of densely packed, perpendicularly aligned high-aspect ratio Pd NNs on ITO substrate via an electrodeposition route. We clarify the factors that have great effect on the size and morphology of the produced Pd NNs and propose a mechanism for the vertically oriented growth of the Pd NNs. We demonstrate that Pd NN arrays can be employed as good SERS substrates due to their unique morphology and orientation.

2. EXPERIMENTAL SECTION

2.1. Materials. Sodium tetrachloropalladate(II) hydrate ($Na_2PdCl_4·3H_2O$), sodium bromide (NaBr), and potassium iodides (KI) were purchased from Alfa Aesar. Trisodium citrate dihydrate ($C_6H_5Na_3O_7·2H_2O$), hydrochloric acid (HCl, 37 wt %), and absolute ethanol were purchased from Beijing Chemical Reagents Co. The *p*-aminothiophenol (PATP) was purchased from Acros Organics. ITO substrates were obtained from Nanbo Co. Ltd. (Shenzhen, China). All chemicals were of analytical grade and used without further purification. All aqueous solutions were prepared with ultrapure water (18 MΩ·cm).

2.2. Synthesis of Pd NCA. All electrochemical experiments were carried out with a CHI 660 electrochemical workstation (CH Instruments, Chenhua Co., Shanghai, China) at room temperature in a conventional three-electrode cell. A saturated calomel electrode (SCE) and a platinum foil were employed as the reference and the counter electrodes, respectively. All potentials were quoted vs SCE. The ITO-coated glass substrates were used as electrodes for electrodeposition because of the following three reasons: (1) the conductivity of ITO substrates is high enough to make them good electrodes. (2) ITO is very stable in the solution within the potential range applied in this work. (3) The ITO substrates are much cheaper than the widely used noble metal and glass carbon electrodes. Before experiments, the ITO substrates were sonicated for 10 and 15 min in 0.5 M KOH and acetone, respectively, and then rinsed with ultrapure water. In a typical electrochemical deposition procedure, double potential step chronoamperometry was employed to deposit Pd nanostructures on ITO substrates in an aqueous solution of 100 mM HCl containing 1.5 mM Na_2PdCl_4, 20 mM NaBr, and 40 mM $C_6H_5Na_3O_7$. The first potential step was used to generate Pd nuclei on ITO by biasing the ITO electrode at −0.400 V for 50 ms, and this step was repeated four times for each sample. The second potential step was used to grow Pd NNs by applying a desired growth potential for certain time. After electrodeposition, the Pd NNs and the Pd NCs modified ITO electrodes were washed with deionized water and dried with high purity nitrogen for other experiments.

2.3. Characterization. The as-prepared Pd NNs and Pd NCs were characterized by field-emission scanning electron microscope (SEM, JSM-6700F, JEOL, Japan, accelerating voltage: 5 kV), transmission electron microscopy (TEM, JEM-2100F, JEOL, Japan, accelerating voltage: 200 kV), XRD (Rigaku X-ray diffractometer, Japan, Cu Kα source, 40 kV, 40 mA), and tapping mode atomic force microscope (AFM, Multimode NanoScope IIIa, Veeco Instruments). For the TEM characterization, the Pd NNs were scraped off from ITO and dispersed in ethanol, and then the resulting solution was dropped onto the carbon film coated copper grid to prepare TEM samples. Raman signals were collected on a HR800 confocal micro-Raman spectrometer (Renishaw plc. UK). Before the SERS measurements, the Pd NNs or Pd NCs modified substrates were immersed into an ethanol solution of 1 mM PATP for 12 h. Each spectrum was collected from 10 different points. The laser power at the surface of the substrate was 30 mW, and the integration time was 10 s. The UV−vis diffuse reflection spectra were obtained from a UV-3600 UV/

dx.doi.org/10.1021/jp500667f | J. Phys. Chem. C 2014, 118, 9758−9768

vis spectrometer (Shimadzu, Japan) with a scan rate of 120 nm/min.

3. RESULTS

3.1. Electrodeposition of Pd NN Arrays. $[PdCl_4]^{2-}$ was used as the precursor in this work, and the main reaction involved in the electrodeposition is

$$[PdCl_4]^{2-} + 2e^- \rightarrow Pd + 4Cl^- \quad (1)$$

The standard redox potential of this reaction is 0.250 V vs SCE. The solution used for electrodeposition in this work contains 1.5 mM $[PdCl_4]^{2-}$ and 100 mM free Cl^-; therefore, the equilibrium potential of the $[PdCl_4]^{2-}$/Pd redox couple in solution was calculated to be 0.385 V on the basis of Nernst equation. Accordingly, the applied potential should be lower than 0.385 V to deposit Pd on ITO substrates. The lower the deposition potential, the larger the deposition driving force, and the faster the deposition rate. To generate Pd nuclei, the ITO substrates were first biased at −0.400 V for 50 ms to produce Pd nuclei on ITO, and this nuclei generation step was repeated four times for each sample. Cyclic voltammograms (CVs) of Pd nuclei modified ITO in different electrolytes were recorded to determine the deposition potentials, and the results are presented in Figure 1.

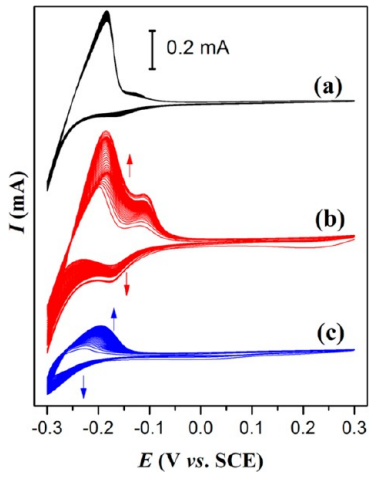

Figure 1. Fifty consecutive CV sweeps of the Pd nuclei modified ITO electrode in (a) 100 mM HCl, (b) 100 mM HCl containing 1.5 mM Na_2PdCl_4, and (c) 100 mM HCl containing 1.5 mM Na_2PdCl_4, 20 mM NaBr, and 40 mM $C_6H_5Na_3O_7$. The geometric area of ITO electrode is 0.21 cm^2, and the potential sweep rate is 50 mV/s.

The Pd nuclei modified ITO electrode exhibits the CV feature of a Pd electrode in 100 mM HCl solution, with a hydrogen adsorption/desorption region from −0.300 to −0.050 V,[41,42] as shown in Figure 1a. After 1.5 mM Na_2PdCl_4 was added to the electrolyte, the hydrogen adsorption/desorption current increases continuously with the increase of potential sweep cycles (Figure 1b), indicating that the total surface area of Pd NCs keep increasing during CV potential sweep. We believe this is due to the growth of Pd NCs by electrochemical reduction of $PdCl_4^{2-}$. As the concentration of $PdCl_4^{2-}$ (1.5 mM) is much lower than that of H^+ (100 mM) in the solution, the reduction current of $PdCl_4^{2-}$ is negligible compared with the current of hydrogen adsorption/desorption. In fact, a reduction wave can be observed in the negatively going potential sweep from ca. 0.300 to 0.100 V in the magnified CV plot of Figure 1b, confirming the electrochemical reduction of $PdCl_4^{2-}$ to Pd.

Bromide and citrate ions have long been utilized as capping agents in the morphology-controlling synthesis of noble metal NCs,[43,44] and they were introduced into the electrolyte to control the growth of Pd NCs in this work. The open-circuit potential of the Pd nuclei modified ITO electrode shifted negatively for tens of millivolts when bromide and citrate were presented in the solution. This phenomenon suggests that the reduction of $PdCl_4^{2-}$ to Pd is greatly retarded by adding capping agents, since a lower potential is now required to reduce the precursor. As presented in Figure 1c, even in the presence of capping agents, the hydrogen adsorption/desorption peaks keep increasing with increasing CV cycles, indicating the electrodeposition of Pd can still occur, but with a lower rate. It should be pointed out here that the hydrogen adsorption/desorption currents drop drastically compared with Figure 1b, implying the hydrogen adsorption and evolution on Pd surface are significantly suppressed by the presence of capping agents. We attribute this phenomenon to the following two reasons: (1) The adsorption of bromide and citrate ions on Pd surface significantly inhibits the adsorption of hydrogen, which is the key step for hydrogen evolution. (2) The growth rate of Pd NCs is significantly lowered due to the presence of capping agent on Pd surface and therefore leading to a much smaller total Pd surface area compared to the Pd NCs grown in the coating-agent-free solution.

For a shape-controlled electrodeposition of metal NCs, it is important to avoid severe hydrogen evolution, which may interfere with the control of the morphology of NCs during deposition. The CV results shown in Figure 1c provide opportunities for shape-controlled growth of Pd NCs via finely tuning the applied potential to modulate the reduction rate of precursor. According to the results shown in Figure 1, the growth of Pd NCs was performed on Pd nuclei modified ITO substrates at potentials ranging from 0.300 to 0.100 V. This deposition potential region was chosen to avoid hydrogen adsorption and evolution, and it was found that Pd NN arrays can be obtained within a narrow potential region from 0.100 to 0.180 V.

3.2. Morphology and Structure Characterization of Electrodeposited Pd NN Arrays. Figure 2a,b shows the typical SEM images of the Pd NNs prepared on ITO substrate by electrodeposition. The low-magnification SEM image (Figure 2a) demonstrates that the Pd NNs grow uniformly in large scale on the substrate. The high-magnification SEM image (Figure 2b) indicates that the Pd nanostructures are high-aspect ratio quadrangular NNs, which are generally perpendicularly oriented to the substrate. Statistics of the Pd NNs in SEM images reveals that they have an average full width at half-maximum (fwhm) of ca. 22 ± 8 nm and a very sharp taper angle at the ends. The vertically aligned NNs construct a highly rough Pd surface. AFM images (Figure S1 in Supporting Information) confirm the rough nature of the Pd NN arrays. In addition, vertically aligned Pd NNs can also be prepared on other conducting substrates such as a sputtered gold film on Si (Figure S2 in Supporting Information), indicating the universal applicability of the deposition method for different substrates.

Figure 2c presents a typical TEM image of Pd NNs, in which two individual nanoneedles are clearly seen. The two Pd NNs have a taper angle of 15° and 16°, respectively. The average taper angle of Pd NNs, which are obtained from several TEM images, is ca. 15 ± 4°. HRTEM was employed to investigate the

dx.doi.org/10.1021/jp500667f | J. Phys. Chem. C 2014, 118, 9758−9768

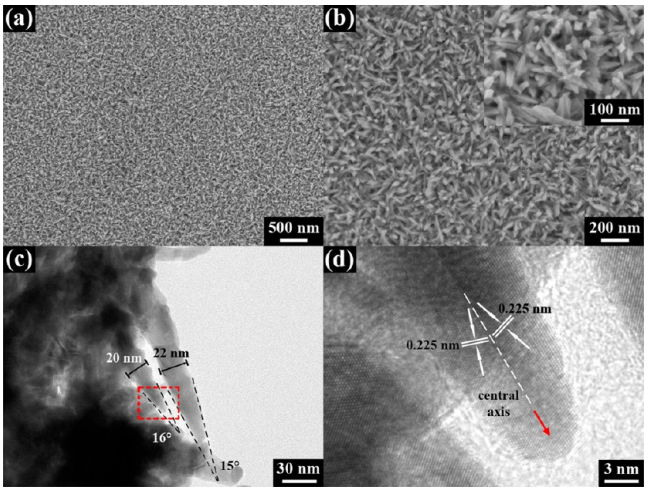

Figure 2. Typical SEM images of Pd NNs in low (a) and high (b) magnification. TEM image of Pd NNs (c) and HRTEM image (d) of the area marked with red dashed square in (c). The Pd NNs were prepared by a four times repeated nucleation process at −0.400 V for 50 ms, followed by a growth process at 0.180 V for 1800 s in 100 mM HCl containing 1.5 mM Na_2PdCl_4, 20 mM NaBr, and 40 mM $C_6H_5Na_3O_7$.

crystal structure of the Pd NNs, and the result is shown in Figure 2d. The Pd NNs exhibit an axial symmetric structure, with the facets stacking symmetrically on both sides of the central axis. The lattice fringe spacing is measured to be 0.225 nm, which corresponds to {111} facets of face-centered cubic Pd crystal. In addition, the width of {111} facets on both sides of the central axis gradually shrink along the direction denoted by the red arrow in Figure 2d, suggesting that each individual nanoneedle is formed through stacking of {111} facets. The XRD pattern of the Pd NN arrays is shown in Figure 3, which

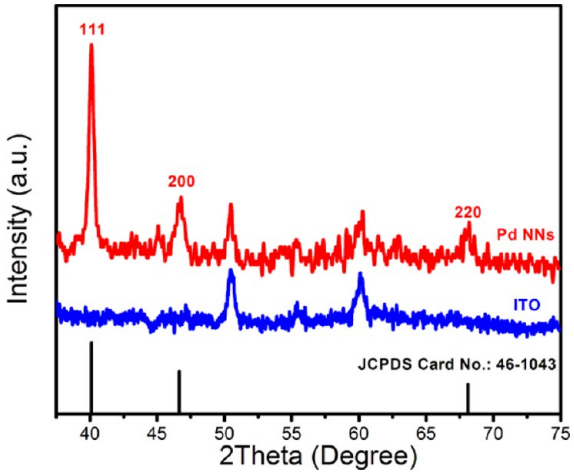

Figure 3. XRD patterns of Pd NN arrays and bare ITO substrate.

demonstrates that the Pd NNs are face-centered cubic (JCPDS 46-1043) crystals. The intensity ratio of the diffraction peak of (111) plane to that of (200) plane is 3.62, which is much higher than that of 1.67 obtained from the JCPDS Card, indicating a preferential [111] orientation. This result is in good agreement with the observations in HRTEM image (Figure 2d). Since most of the Pd NNs are almost perpendicularly oriented to the substrate, the {111} facet groups have the largest diffraction area among all facet groups in the XRD measurements. As a result, the {111} facets exhibit the highest intensity in the XRD pattern. By combining XRD, SEM, and TEM results, it can be concluded that Pd NNs grow through the stacking of {111} facets.

3.3. Effect of the Prenucleation Step on the Growth of Pd NNs. As mentioned above, a two-step electrodeposition was used to grow Pd NNs. The first step was a prenucleation step performed at a very low potential for extremely short time, in which large amount of very small Pd nuclei were generated on ITO substrates. These nuclei serve as active nanoseeds in the following growth step. Since the time duration of the prenucleation step was extremely short (50 ms), the formed Pd nuclei were too small to be identified in SEM or AFM images even with very high magnification.[34] However, if this step was repeated for more than 10 times, numerous uniformly dispersed Pd nanoseeds could be observed in SEM images (Figure S3 in Supporting Information), providing solid evidence that biasing ITO at −0.400 V can generate large amount of Pd nuclei. To illustrate the importance of the prenucleation step, Pd NNs were prepared with and without this step. Figure 4 shows the typical SEM images of Pd NNs

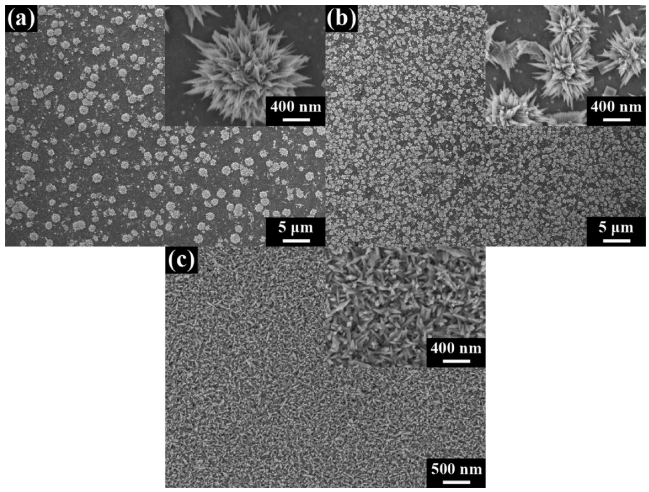

Figure 4. SEM images of Pd NNs prepared by electrodeposition at 0.180 V for 1800 s in 100 mM HCl containing 1.5 mM Na_2PdCl_4, 20 mM NaBr, and 40 mM $C_6H_5Na_3O_7$: (a) without a nucleation step, (b) with a four times repeated nucleation step at −0.100 V for 50 ms, and (c) with a four times repeated nucleation step at −0.400 V for 50 ms.

prepared without the prenucleation step and with the prenucleation step but at different nanoseed-generating potentials. Figure 4a clearly shows that skipping the prenucleation step results in the formation of sporadically dispersed urchin-like nanostructures, which are composed of randomly oriented Pd NNs. This result indicates that the nanoseed-generating step plays a key role in determining the morphology and growth density of the Pd NNs.

In addition, the nucleation potential is also critical to the formation of well-aligned Pd NNs. The lower the nucleation potential, the larger the driving force for creating Pd nuclei by precursor reduction, and then the high nuclei density on the substrate. As shown in Figure 4b, when the prenucleation was conducted at −0.100 V, the resulting Pd NNs also exhibit a habit of growing in urchin-like groups, and the density of NNs groups increases greatly compared to those without the prenucleation step. When the ITO substrate was biased at

dx.doi.org/10.1021/jp500667f | J. Phys. Chem. C 2014, 118, 9758−9768

−0.400 V to generate Pd nuclei, well-aligned Pd NN arrays were obtained after the growth step (Figure 4c). Further negatively shifting the nucleation potential will lead to a peeling-off of the Pd NN arrays. This is due to the extremely high nuclei density, which results in large lateral stress among NNs during the growth process. It should be mentioned that the duration of prenucleation should be extremely short, since longer time may lead to a progressive nucleation, which causes a wide size dispersity of the nanoseeds and finally leads to a nonuniformity in the size of Pd NNs.

3.4. Effect of the Electrodeposition Potential on the Growth of Pd NNs. The second electrodeposition step, which was performed at low deposition overpotentials (small deposition driving force), was a mild process for the growth of Pd NNs from nanoseeds. It was found in earlier work that the substrate potential is critical to the morphology and size of the metal NCs prepared by electrodeposition,[32−34,45] and there is usually a narrow potential range within which anisotropic growth of metal NCs can be achieved.[34] To determine the potential window for anisotropic growth of Pd NCs, different potentials were applied to the nanoseed-modified ITO substrates. Figure 5 displays the potential-dependent morphology evolution of the as-prepared Pd NCs. When the growth potential was equal to or larger than 0.300 V, isotropic Pd NCs with low growth density and wide size distribution were obtained (Figure 5a,b). When the growth potential was lowered to 0.250 V, flower-shaped particles were produced, as shown in Figure 5c. Each "flower" was composed of many nanopyramids, implying the beginning of anisotropic growth. As the potential is further decreased to 0.200 V, the aspect ratio of the nanopyramids increases, leading to the formation of well-defined Pd NNs (Figure 5d). Further negatively shifting the growth potential to 0.180, 0.150, and 0.100 V can increase the aspect ratio of Pd nanoneedles (Figure 2a,b and Figure S4 in Supporting Information). It should be pointed out here that, within the potential region of 0.200−0.320 V, the adhesion of the Pd NNs to the ITO substrate is strong enough to survive sonication in water.

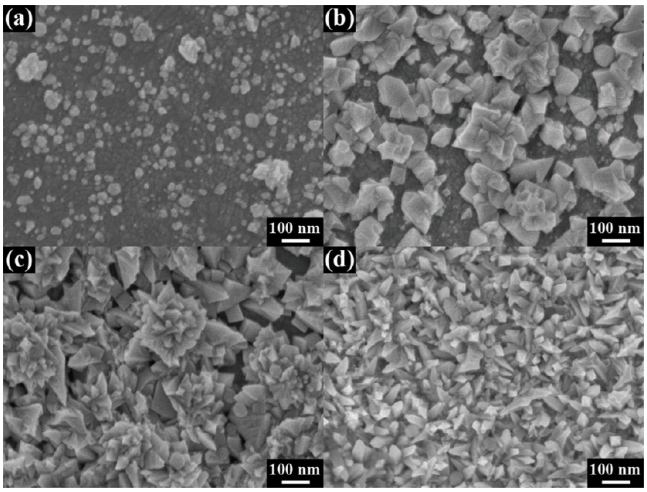

Figure 5. SEM images of Pd NCs prepared by a four times repeated nucleation process at −0.400 V for 50 ms, followed by a growth process at different potentials for 1800 s in 100 mM HCl containing 1.5 mM Na_2PdCl_4, 20 mM NaBr, and 40 mM $C_6H_5Na_3O_7$: (a) 0.320, (b) 0.300, (c) 0.250, and (d) 0.200 V.

If the growth potential was decreased below 0.100 V, Pd NNs were no longer obtained due to the fast isotropic deposition of Pd under large driving force, and the resulting Pd film usually peeled off from ITO substrate due to the lateral stress among large Pd NCs. These results not only provide direct evidence that the growth potential is a key factor controlling the size and morphology of Pd NCs but also confirm the existence of a narrow potential range from 0.100 to 0.200 V, in which vertically aligned Pd NNs can be obtained. The synergic effect of the potential-determined reduction rate of the precursor and the potential-related adsorption/desorption behavior of the capping agents is believed to be responsible for the formation of Pd NNs, and the detailed mechanism will be discussed in section 4.1.

3.5. Effect of the Bromide and Citrate on the Growth of Pd NNs. Capping agents such as small anions and surfactants have long been used to direct the growth of NCs and control their morphology via selectively interacting with certain facets of metal NCs and then modulating their growth rates.[46] Figure 6a−c shows the SEM images of Pd NCs prepared in electrolytes with different bromide concentrations. Low-aspect-ratio Pd nanopyramids with low growth density are produced in the absence of bromide (Figure 6a), whereas in the presence of bromide, well-defined Pd NNs with smooth surface are obtained (Figure 6b,c), indicating the importance of Br^- in shaping Pd NNs. Moreover, the fwhm of Pd NNs decreases slightly with increasing Br^- concentration. It should be pointed out that when Br^- concentration exceeds 80 mM, vertically aligned Pd NN arrays can no longer be obtained, as shown in Figure S5 of the Supporting Information. These results indicate that there exists an appropriate concentration range of bromide for producing well-aligned and densely packed Pd NNs. Replacing bromide with other small anion will completely change the morphology of the Pd NCs. For example, Pd nanocubes are the dominant products when there is trace amount of I^- (0.04 mM) present in the solution (Figure 6d), demonstrating the irreplaceable role of bromide for the formation of Pd NN arrays.

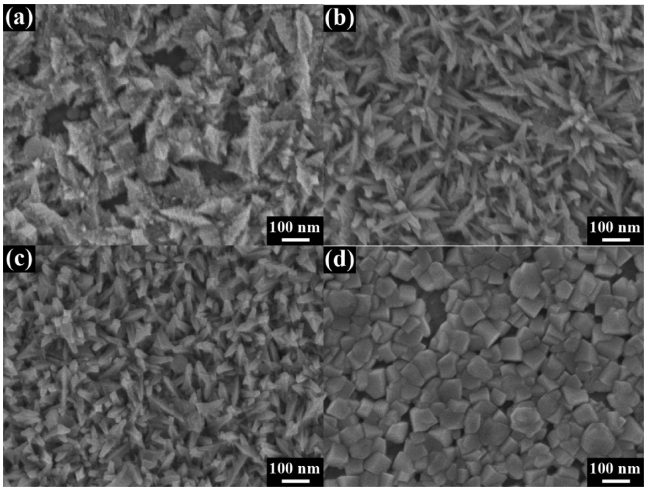

Figure 6. SEM images of Pd NCs prepared by a four times repeated nucleation process at −0.400 V for 50 ms, followed by a growth process at 0.180 V for 1800 s in 100 mM HCl containing 1.5 mM Na_2PdCl_4, 40 mM $C_6H_5Na_3O_7$, and different concentrations of NaBr or KI: (a) 0 mM NaBr, (b) 10 mM NaBr, (c) 40 mM NaBr, and (d) 0.04 mM KI.

dx.doi.org/10.1021/jp500667f | J. Phys. Chem. C 2014, 118, 9758−9768

Citrate binds most strongly to the {111} facets of Pd and has been used as capping agent to control the shape of Pd NCs.[44,46,47] The effect of citrate on the growth of Pd NNs was also investigated in this work, and the results are shown in Figure 7. Without citrate ions in the deposition solution, Pd

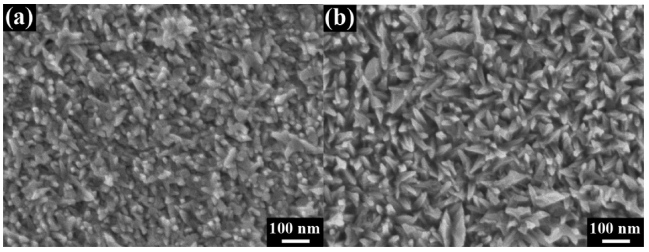

Figure 7. SEM images of Pd NCs prepared in the absence (a) and presence (b) of 20 mM $C_6H_5Na_3O_7$ in 100 mM HCl containing 1.5 mM Na_2PdCl_4 and 20 mM NaBr.

NCs with irregular shapes dominates the products, implying that the presence of citrate is also a requisite condition for the formation of well-aligned Pd NNs. However, unlike bromide, the concentration of citrate has little influence on the morphology of the final product (Figure S6 in the Supporting Information). It can be inferred from these phenomena that citrate ions play an assistant role in shaping Pd NNs. The detailed mechanism of the effects of bromide and citrate on the morphology of Pd NCs will be described in the Discussion section.

3.6. Effect of the Electrodeposition Time on the Orientation of Pd NNs. The morphology and orientation of Pd NCs were also investigated with the variation of electrodeposition time, and the results are shown in Figure 8. In the first 120 s of electrodeposition, most of the Pd nanoseeds exhibit a growth tendency to form a preliminary thorny structure, as can be seen in Figure 8a. After deposition for 300 s, a group of nanothorns protrude from the nanoseeds, and there is no evidence of oriented growth since the nanothorns grow along various directions (Figure 8b). When the growth time is increased to over 600 s, Pd NNs start to show a preferential growth direction that is perpendicular to the substrate, as shown in Figure 8c and Figure 2a,b. However, when the growth time is longer than 2400 s, the obtained Pd NN film peeled off from ITO substrates due to the lateral stress between adjacent NNs. Therefore, the best deposition duration for perpendicularly oriented Pd NNs is ca. 20−30 min.

3.7. Pd NN Arrays as Active SERS Substrates. The SERS activity of the Pd NNs and nanocubes was examined under 488 nm excitation, using *p*-aminothiophenol (PATP) as the probe molecule, and the results are shown in Figure 9a. The spectra present the fingerprint features of PATP with main peaks located at around 1079 and 1586 cm^{-1}, while the 1146, 1392, and 1444 cm^{-1} peaks come from the 4,4′-dimercaptoazobenzene, a resultant of the oxidation of PATP catalyzed by Pd NCs.[48] The peak assignment according to literatures[48−50] is listed in Table 1. The νCS vibration peak shifts from 1084 cm^{-1} of bulk PATP to 1079 cm^{-1} (or 1075 cm^{-1}) in the SERS spectra, indicating the formation of a Pd−S bond. This peak exhibits smaller enhancement than that of 1589 cm^{-1}, possibly because the vertical alignment of PATP molecule on Pd has greater influence on the stretch of C−S bond.[51,52]

The enhancement factor (EFs) of Pd NNs and nanocubes were calculated using the equation[4]

$$\mathrm{EF} = (I_{\mathrm{SERS}}/N_{\mathrm{ads}})/(I_{\mathrm{bulk}}/N_{\mathrm{bulk}}) \quad (2)$$

in which I_{SERS} and I_{bulk} are intensities of the same peak from the SERS and Raman spectrum, respectively. N_{ads} is the number of adsorbed PATP molecules on the Pd NNs (or nanocubes) within the laser irradiated area, while N_{bulk} is the number of molecules in bulk PATP illuminated by the laser. Taking the 1589 cm^{-1} peak for calculation, I_{bulk} is 1125.6, and I_{SERS} for Pd NNs and nanocubes are 416.9 and 179.3, respectively. The surface area occupied by individual adsorbed PATP molecule is about 0.20 nm^2,[53] and therefore, N_{ads} is estimated to be 3.5×10^7 and 4.6×10^7 for Pd NNs and nanocubes, respectively. N_{bulk} is calculated to be 2.05×10^{11} under 488 nm excitation.[51] Therefore, the EF values of Pd NNs and nanocubes are calculated to be 2.2×10^3 and 7.1×10^2, respectively. It should be mentioned here that SERS spectra obtained on Pd substrates using 488 nm excitation are rarely reported. The EF value obtained in this work is comparable with previous work using PATP as probing molecules and the 632 nm laser as excitation source. This result indicates that Pd NN arrays can be used as a promising SERS substrate candidate. In addition, Pd NNs also exhibited SERS activities under UV (325 nm) excitation; however, the EF is much lower than that obtained under 488 nm excitation (Figure S7 in Supporting Information).

4. DISCUSSION

4.1. Mechanism of How the Capping Agent and the Deposition Potential Influence the Growth of Pd NNs. The growth of noble metal NCs in equilibrium conditions depends greatly on the thermodynamic conditions of different facets. For face-centered cubic metal crystals, the surface energies (denoted as γ) of different crystallographic facets usually decrease in the order of $\gamma_{\{110\}} > \gamma_{\{100\}} > \gamma_{\{111\}}$;[54,55] thus,

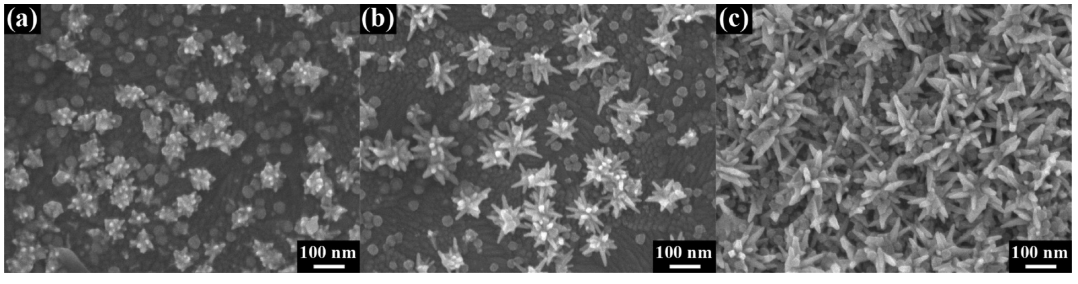

Figure 8. SEM images of Pd NCs prepared by a four times repeated nucleation process at −0.400 V for 50 ms, followed by a growth process at 0.180 V for different time: (a) 120, (b) 300, and (c) 600 s. The deposition solution is 100 mM HCl containing 1.5 mM Na_2PdCl_4, 20 mM NaBr, and 40 mM $C_6H_5Na_3O_7$.

dx.doi.org/10.1021/jp500667f | J. Phys. Chem. C 2014, 118, 9758−9768

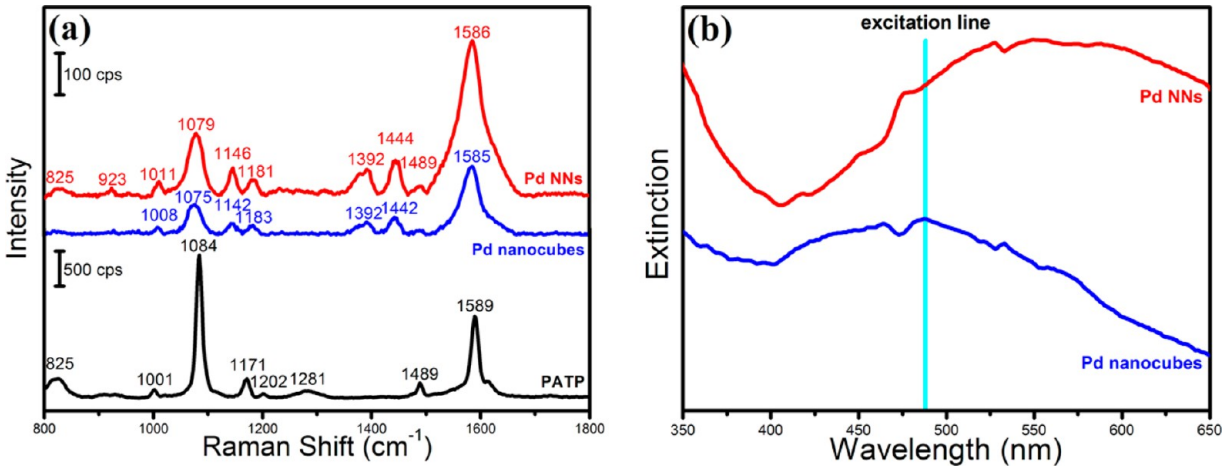

Figure 9. (a) SERS spectra of Pd NNs and nanocubes and Raman spectrum of bulk PATP. (b) UV–vis spectra of Pd NNs and nanocubes.

Table 1. Raman Band Frequencies of PATP

Pd NNs (cm^{-1})	Pd nanocubes (cm^{-1})	bulk PATP (cm^{-1})	assignment[a]
825		825	πCH, 11 (b_1)
923			πCH, 5b (b_1)
1011	1008	1001	γCC + γCCC, 18a (a_1)
1079	1075	1084	νCS, 7a (a_1)
1181	1183	1171	δCH, 9a (a_1)
		1202	
		1281	νCH, 7a′ (a_1)
1489	1489	1489	νCC + δCH, 19a (a_1)
1586	1585	1589	νCC, 8a (a_1)

[a] ν, stretch; δ and γ, bend; π, wagging. Letters in parentheses indicate the vibrational symmetry.

particles enclosed mainly by {111} and {100} facets are the most thermodynamically stable,[46] and the final shape of nanocrystals in a thermodynamic growth is determined by the percentages of these two facets in all the exposed ones. Usually, a kinetic-controlled regime is preferred in the anisotropic growth of metal NCs, and this regime can be achieved by slowing down the reduction rate of the precursor.[56] Bromide and citrate can preferentially bind to the {100} and {111} facets of Pd, respectively, and therefore reduce the growth rates of these facets.[57] Since the facets that grow slower tend to be preserved in the resulting product, the addition of capping agents to deposition solution has remarkable effects on the morphology of Pd NCs.

Bromide ions have two main roles in the formation of NNs. The first role is to replace chloride ions in the complex of $[PdCl_4]^{2-}$ and yield $[PdCl_{4-n}Br_n]^{2-}$, whose reduction rate is slower than that of $[PdCl_4]^{2-}$.[58−60] The second role of Br^- is to act as a capping agent during the electrochemical growth of Pd NCs. From the HRTEM image shown in Figure 2d, a twined NC boundary marked by the dashed line is clearly seen in the middle of a nanoneedle, and therefore the nanoneedle is an elongated nanopyramid grown from a single twined nanoseed.[57] The selective adsorption of Br^- on (100) facets slows down the growth rate of (100) facets and thus favors the formation of pyramid structure with (100) as the exposed facets.[43,61] However, if too much Br^- was added to electrolyte, the nucleation and growth of Pd NCs would be more difficult, resulting in the sharp decrease of the growth density of Pd NCs (see Figure S5 in Supporting Information). Moreover, with a large amount of excessive Br^- in solution, not only (100) but also other facets were coated with bromide. This greatly reduces the difference in growth rate among different facets and leading to the formation of Pd nanopyramids with a low aspect ratio (Figure S5 in Supporting Information). This explains why there exists a proper concentration range of Br^- for the electrodeposition of Pd NN arrays.

Citrate acts as a capping agent during electrodeposition of Pd NCs. It has been demonstrated that citrate binds more strongly to the {111} facets of Pd crystals,[37,39,40] thus favoring the formation of Pd NCs enclosed by {111} facets, such as octahedra, icosahedra, and decahedra. Previous work showed that citrate adsorbs on noble metals via three $-COO^-$ groups, and even citric acid deprotonates fully upon adsorption.[62] However, in this work, the most of the citrate ions were protonated due to the acid nature of 100 mM HCl solution, and the citrate could not form a dense adsorption layer on the {111} facets of Pd. As a result, the growth rate of the {111} facets is faster than that of the Br^- coated {100} facets, leading to the formation of the high-aspect-ratio pyramid structure. This implies the assistant role of citrate in shaping Pd NCs in acid solution.

The applied potential plays a dual role in determining the morphology of Pd NCs during electrodeposition. First, it determines the reduction rate of the precursor. The lower the substrate potential, the larger the driving force for the reduction of the precursor and thus the faster growth rate of Pd NCs. Second, the applied potential significantly influences the adsorption/desorption behavior of the capping agents. The citrate-related species are negatively charged when they are adsorbed on noble metals because all three carboxylic acid groups are deprotonated upon adsorption even in acid solution.[62,63] Therefore, the adsorption behaviors of both the citrate-related species and the bromide ions are inevitably affected by the potential applied to the electrode. It is more difficult for the negatively charged citrate-related species and Br^- to adsorb on the noble metal surfaces when the applied potential is negatively shifted.[32,64] Considering the intrinsic adsorption behaviors of citrate and Br^- on different facets, it is possible to enlarge the difference in the compactness of adsorbed layer on different facets by tuning the applied potential. In other words, it is possible, by controlling potential,

dx.doi.org/10.1021/jp500667f | J. Phys. Chem. C 2014, 118, 9758−9768

to block certain crystal facets via capping agent adsorption while leaving others still accessible to the precursor.

At high potentials such as 0.300 V or above, the two negatively charged capping agents (citrate and Br^-) binded firmly with almost all facets of Pd NCs. The growth rates of different facets were very low and close to each other. As a result, isotropic Pd NCs with {100} and {111} as the dominant exposed facets were obtained, and the growth density of Pd NCs was very low (Figure 5a,b). As the potential was negatively shifted, to 0.250 V, the {111} facets, which were mainly coated by citrate, were accessible to the precursor because of the partial desorption of citrate. The difference in growth rate between {111} and {100} facets increases, leading to an anisotropic growth trend for Pd NCs (Figure 5c). When the potential is further decreased to 0.200 V or below, the anisotropic growth of Pd NCs became more obvious, and as a result, high-aspect-ratio nanoneedles were formed as the dominant products (Figure 5d, Figure 2a,b, and Figure S4 in Supporting Information). However, if the potential was too low, both citrate and Br^- desorbed from Pd NCs, and the fast reduction of the precursor led to the formation of larger Pd NCs and the poor mechanical stability. Therefore, the substrate potential in the electrodeposition is critical to the morphology of Pd NCs. Only when the potential is in a proper range, i.e. from 0.100 to 0.200 V, can well-defined Pd NNs be produced.

4.2. Mechanism for Oriented Growth. The schematic representation of the mechanism of oriented growth is shown in Scheme 1. The Pd nanoseeds were first produced on the ITO substrate during the high-overpotential nanoseed-generating step (Scheme 1a). In the following growth step, Pd NNs were obtained with the help of capping agents and applied potential. However, not all Pd nanoseeds finally grew into Pd NNs, and some of them did not exhibit a growth tendency to form NN structure, as can be seen clearly in Figure 8. We believe this is due to the structural difference of nanoseeds. As is confirmed by previous works,[57,61] the nanoseeds could be single, single twined, and multiple twined crystals, and the final morphology of metal nanocrystals is highly dependent on the structure of the nanoseeds. The shapes of the nanocrystals grown from different structured nanoseeds are sure to be quite different. The HRTEM image (Figure 2d) indicates the Pd NNs were grown from single twined nanoseeds. Therefore, the Pd nanoseeds that have different structure with single twined nanoseeds may not finally grow into Pd NNs.

Scheme 1. Growth Mechanism of Vertically Oriented Pd Nanoneedles

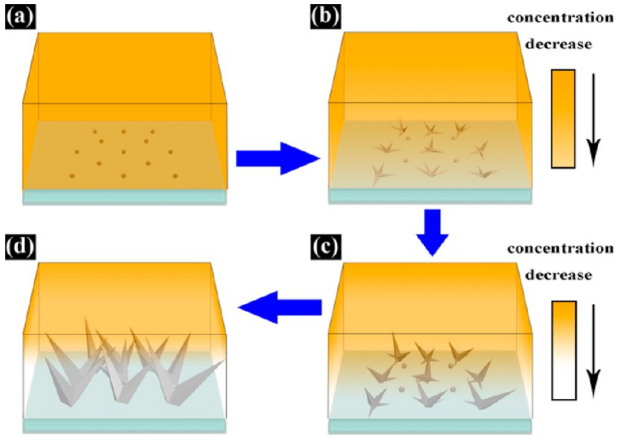

The Pd NNs are randomly oriented in the initial growth stage, as shown in Scheme 1b. The high growth density results in the overlap of the diffusion layers of adjacent Pd NNs, which generates a uniform diffusion layer on the ITO electrode surface.[65] With electrodeposition going on, the concentration gradient of the precursor within the diffusion layer is increased. In other words, the closer to the ITO substrates, the lower the concentration of precursor. Because of the difference in concentration along the direction vertical to the ITO, more $[PdCl_4]^{2-}$ ions reach the top of the standing Pd NNs, and the standing Pd NNs grow much faster than those lying on the substrate. Moreover, the development of the diffusion layer may lead to the presence of a depletion layer on the ITO/solution interface, which will completely stop the growth of the laying Pd NNs. Therefore, the diffusion layer is preferential for the growth of standing Pd NNs, and the vertically aligned Pd NNs are the main product after long time electrodeposition (Scheme 1d). It should be pointed herein that the applied potential also plays an important role in the vertical growth of Pd NNs since it not only governs the reduction rate of precursor but also influences the concentration gradient of $[PdCl_4]^{2-}$. Vertically aligned Pd NNs can only be prepared within the potential region from 0.100 to 0.200 V. As is discussed in sections 3.4 and 4.1, the reduction driving force and the consumption rate of $[PdCl_4]^{2-}$ are very low at high potentials (>0.200 V), and therefore the concentration gradient of precursor can hardly develop under this condition. Then, vertically aligned Pd NNs are not produced as the main product (see Figure 5). When the applied potential is too low (<0.100 V), the fast reduction rate results in an isotropic growth of Pd nanocrystals, and no Pd NNs can be obtained.

4.3. Mechanism for SERS Enhancement. SERS activity of metal NCs is significantly related to their chemical composition,[66] shape,[18] size, spacing between adjacent particles,[67] and excitation wavelength as well.[68] It can be inferred that electromagnetic enhancement is the dominant enhancement mechanism in this work since most of the peaks show an a_1 vibration mode.[51] It is well accepted that there are three effects that contribute to the electromagnetic enhancement: the image dipole enhancement effect, the surface plasmonic effect, and the lightning-rod effect[69] that increases the local electromagnetic field. The surface plasmon resonance bands of Pd NNs and nanocubes were compared using UV−vis spectroscopy, and the result is shown in Figure 9b. The centers of the plasmonic bands for Pd NNs and Pd nanocubes are around 550 and 487 nm, respectively, with the latter closer to the excitation light of 488 nm. Therefore, the resonance excitation contribution of Pd nanocubes to SERS is greater than that of Pd NNs. As for the lighting-rod effect,[70] however, the contribution of local field enhancement to SERS on Pd NNs is much larger than that on Pd nanocubes because the sharp top ends of Pd NNs can more efficiently enhance the local electromagnetic field. Moreover, the vertical orientation of Pd NNs further increases the interaction of excitation light with the sharp ends of NNs. Thus, it is not difficult to understand why Pd NNs show a greater enhancement than Pd nanocubes. It should be pointed out here that we believe the enhancement effect of Pd NNs may be further improved by enhancing the plasmonic effect via tuning the excitation light closer to the maximum resonance wavelength of Pd NNs (for example, 633 nm laser). The uniformity of the SERS signals on Pd NNs and

dx.doi.org/10.1021/jp500667f | J. Phys. Chem. C 2014, 118, 9758−9768

nanocubes was also evaluated by calculating the relative standard deviations (RSDs) of the intensity of the two main peaks. The RSDs of 1079 and 1586 cm^{-1} peak on Pd NNs are 44.5% and 42.1%, respectively. Though these values are acceptable, they are much larger than the values on Pd nanocubes (14.9% and 6.5%). This result implies that Pd nanocubes exhibit better SERS uniformity than Pd NNs. We believe that the relatively high RSD of Pd NNs is due to their unique structure. The top ends of Pd NNs serve as SERS "hot spots" due to the lighting-rod effect. As the orientation of Pd NNs is not strictly identical, the number of the SERS hot spots within the laser irradiated area varies from point to point, leading to a relative high RSD value.

5. CONCLUSIONS

Densely packed standing high-aspect-ratio Pd NNs with fwhm of 22 ± 8 nm and taper angle of 15 ± 4° were successfully deposited on ITO surfaces via a facile two-step electrodeposition route. The first step, which was conducted under a highly negative overpotential for an extremely short time to generate Pd nanoseeds, is indispensable for the uniform growth of Pd NNs. The applied potential in the following growth step is critical for modulating the shape of Pd nanoparticles, and the vertically aligned Pd NNs can only be produced within a narrow potential window from 0.100 to 0.200 V. The presence of bromide and citrate ions is another key point for the formation of Pd NNs, and Br^- plays a dominant role in shaping Pd NCs via forming a complex with the precursor and selective adsorption on the {100} facets. XRD and HRTEM results indicate that the Pd NNs were formed through the stacking of {111} facets. We believe that the concentration gradient of precursor in the diffusion layer plays a key role in the vertically oriented growth of Pd NNs. The Pd NNs exhibit higher SERS activity compared to Pd nanocubes, demonstrating their potential application as SERS-active substrates. We believe that the unique morphology with sharp vertices and the perpendicular alignment of Pd NNs are responsible for their SERS performance.

■ ASSOCIATED CONTENT

Supporting Information

AFM images of Pd nanoneedles, SEM images of Pd nanoseeds, SEM images of Pd nanoneedles prepared on sputtered Au film, SEM images of Pd nanoneeles prepared under lower growth potentials or higher NaBr concentration, and Raman spectra under the excitation of 325 nm laser. This material is available free of charge via the Internet at http://pubs.acs.org.

■ AUTHOR INFORMATION

Corresponding Author

*Tel +86 01 82339562; Fax +86 01 82339562; e-mail pdiao@buaa.edu.cn (P.D.).

Notes

The authors declare no competing financial interest.

■ ACKNOWLEDGMENTS

We gratefully acknowledge the financial support of this work by National Natural Science Foundation of China (NSFC 21173016 and 20973020), Beijing Natural Science Foundation (2142020), and Doctoral Fund of Ministry of Education of China (20101102110002).

■ ABBREVIATIONS

NNs, nanoneedles; ITO, indium tin oxide; fwhm, full width at half-maximum; XRD, X-ray diffraction; HRTEM, high-resolution transmission electron microscopic; NCs, nanocrystals; SEM, scanning electron microscopic; SERS, surface-enhanced Raman scattering; PATP, *p*-aminothiophenol; SCE, saturated calomel electrode; TEM, transmission electron microscopy; AFM, atomic force microscope; CVs, cyclic voltammograms; EF, enhancement factor.

■ REFERENCES

(1) Chen, Y. H.; Hung, H. H.; Huang, M. H. Seed-Mediated Synthesis of Palladium Nanorods and Branched Nanocrystals and Their Use as Recyclable Suzuki Coupling Reaction Catalysts. *J. Am. Chem. Soc.* **2009**, *131*, 9114−9121.

(2) Surendran, G.; Ksar, K.; Ramos, L.; Keita, B.; Nadjo, L.; Prouzet, E.; Beaunier, P.; Dieudonne, P.; Audonnet, F.; Remita, H. Palladium Nanoballs Synthesized in Hexagonal Mesophases. *J. Phys. Chem. C* **2008**, *112*, 10740−10744.

(3) Zeng, X. Q.; Latimer, M. L.; Xiao, Z. L.; Panuganti, S.; Welp, U.; Kwok, W. K.; Xu, T. Hydrogen Gas Sensing with Networks of Ultrasmall Palladium Nanowires Formed on Filtration Membranes. *Nano Lett.* **2011**, *11*, 262−268.

(4) McLellan, J.; Xiong, Y.; Hu, M.; Xia, Y. Surface-Enhanced Raman Scattering of 4-Mercaptopyridine on Thin Films of Nanoscale Pd Cubes, Boxes, and Cages. *Chem. Phys. Lett.* **2006**, *417*, 230−234.

(5) Yang, F.; Kung, S.-C.; Cheng, M.; Hemminger, J. C.; Penner, R. M. Smaller is Faster and More Sensitive: The Effect of Wire Size on the Detection of Hydrogen by Single Palladium Nanowires. *ACS Nano* **2010**, *4*, 5233−5244.

(6) Diao, P.; Zhang, D. F.; Guo, M.; Zhang, Q. Electrocatalytic Oxidation of CO on Supported Gold Nanoparticles and Submicroparticles: Support and Size Effects in Electrochemical Systems. *J. Catal.* **2007**, *250*, 247−253.

(7) Chen, A. C.; Holt-Hindle, P. Platinum-Based Nanostructured Materials: Synthesis, Properties, and Applications. *Chem. Rev.* **2010**, *110*, 3767−3804.

(8) Kim, F.; Connor, S.; Song, H.; Kuykendall, T.; Yang, P. D. Platonic Gold Nanocrystals. *Angew. Chem., Int. Ed.* **2004**, *43*, 3673−3677.

(9) Li, C.; Shuford, K. L.; Chen, M.; Lee, E. J.; Cho, S. O. A Facile Polyol Route to Uniform Gold Octahedra with Tailorable Size and Their Optical Properties. *ACS Nano* **2008**, *2*, 1760−1769.

(10) Lee, H.; Habas, S. E.; Kweskin, S.; Butcher, D.; Somorjai, G. A.; Cubic, P. Y. Morphological Control of Catalytically Active Platinum Nanocrystals. *Angew. Chem., Int. Ed.* **2006**, *45*, 7824−7828.

(11) Cheong, S.; Watt, J.; Ingham, B.; Toney, M. F.; Tilley, R. D. In Situ and Ex Situ Studies of Platinum Nanocrystals: Growth and Evolution in Solution. *J. Am. Chem. Soc.* **2009**, *131*, 14590−14595.

(12) Sun, Y. G.; Xia, Y. N. Shape-Controlled Synthesis of Gold and Silver Nanoparticles. *Science* **2002**, *298*, 2176−2179.

(13) Tao, A.; Sinsermsuksakul, P.; Yang, P. Polyhedral Silver Nanocrystals with Distinct Scattering Signatures. *Angew. Chem., Int. Ed.* **2006**, *45*, 4597−4601.

(14) Zhang, Y.; Grass, M. E.; Habas, S. E.; Tao, F.; Zhang, T.; Yang, P.; Somorjai, G. A. One-Step Polyol Synthesis and Langmuir−Blodgett Monolayer Formation of Size-Tunable Monodisperse Rhodium Nanocrystals with Catalytically Active (111) Surface Structures. *J. Phys. Chem. C* **2007**, *111*, 12243−12253.

(15) Zettsu, N.; McLellan, J. M.; Wiley, B.; Yin, Y.; Li, Z.-Y.; Xia, Y. Synthesis, Stability, and Surface Plasmonic Properties of Rhodium Multipods, and Their Use as Substrates for Surface-Enhanced Raman Scattering. *Angew. Chem., Int. Ed.* **2006**, *45*, 1288−1292.

(16) Huang, X. Q.; Zheng, N. F. One-Pot, High-Yield Synthesis of 5-Fold Twinned Pd Nanowires and Nanorods. *J. Am. Chem. Soc.* **2009**, *131*, 4602−4603.

(17) Niu, W. X.; Li, Z. Y.; Shi, L. H.; Liu, X. Q.; Li, H. J.; Han, S.; Chen, J. A.; Xu, G. B. Seed-Mediated Growth of Nearly Monodisperse Palladium Nanocubes with Controllable Sizes. *Cryst. Growth Des.* **2008**, *8*, 4440−4444.
(18) Fan, F. R.; Attia, A.; Sur, U. K.; Chen, J. B.; Xie, Z. X.; Li, J. F.; Ren, B.; Tian, Z. Q. An Effective Strategy for Room-Temperature Synthesis of Single-Crystalline Palladium Nanocubes and Nanodendrites in Aqueous Solution. *Cryst. Growth Des.* **2009**, *9*, 2335−2340.
(19) Xiong, Y. J.; McLellan, J. M.; Chen, J. Y.; Yin, Y. D.; Li, Z. Y.; Xia, Y. N. Kinetically Controlled Synthesis of Triangular and Hexagonal Nanoplates of Palladium and Their SPR/SERS Properties. *J. Am. Chem. Soc.* **2005**, *127*, 17118−17127.
(20) Niu, Z. Q.; Peng, Q.; Gong, M.; Rong, H. P.; Li, Y. D. Oleylamine-Mediated Shape Evolution of Palladium Nanocrystals. *Angew. Chem., Int. Ed.* **2011**, *50*, 6315−6319.
(21) Xiong, Y. J.; Chen, J. Y.; Wiley, B. J.; Xia, Y. N.; Aloni, S.; Yin, Y. D. Understanding the Role of Oxidative Etching in the Polyol Synthesis of Pd Nanoparticles with Uniform Shape and Size. *J. Am. Chem. Soc.* **2005**, *127*, 7332−7333.
(22) Valden, M.; Lai, X.; Goodman, D. W. Onset of Catalytic Activity of Gold Clusters on Titania with the Appearance of Nonmetallic Properties. *Science* **1998**, *281*, 1647−1650.
(23) Yoon, B.; Hakkinen, H.; Landman, U.; Worz, A. S.; Antonietti, J.-M.; Abbet, S.; Judai, K.; Heiz, U. Charging Effects on Bonding and Catalyzed Oxidation of CO on Au_8 Clusters on MgO. *Science* **2005**, *307*, 403−407.
(24) Erikson, H.; Sarapuu, A.; Tammeveski, K.; Solla-Gullón, J.; Feliu, J. M. Enhanced Electrocatalytic Activity of Cubic Pd Nanoparticles Towards the Oxygen Reduction Reaction in Acid Media. *Electrochem. Commun.* **2011**, *13*, 734−737.
(25) Diao, P.; Zhang, D.; Wang, J.; Zhang, Q. Electrocatalytic Activity of Supported Gold Nanoparticles toward CO Oxidation: the Perimeter Effect of Gold-Support Interface. *Electrochem. Commun.* **2010**, *12*, 1622−1625.
(26) Yuan, J. H.; Wang, K.; Xia, X. H. Highly Ordered Platinum-Nanotubule Arrays for Amperometric Glucose Sensing. *Adv. Funct. Mater.* **2005**, *15*, 803−809.
(27) Wang, J. Y.; Diao, P.; Zhang, D. F.; Xiang, M.; Zhang, Q. Electrochemical Sensing of CO by Gold Particles Electrodeposited on Indium Tin Oxide Substrate. *Electrochem. Commun.* **2009**, *11*, 1069−1072.
(28) Wang, J.; Diao, P.; Zhang, Q. Dual Detection Strategy for Electrochemical Analysis of Glucose and Nitrite Using a Partitionally Modified Electrode. *Analyst* **2012**, *137*, 145−152.
(29) Hanauer, M.; Pierrat, S.; Zins, I.; Lotz, A.; Sönnichsen, C. Separation of Nanoparticles by Gel Electrophoresis According to Size and Shape. *Nano Lett.* **2007**, *7*, 2881−2885.
(30) Tian, N.; Zhou, Z.-Y.; Sun, S.-G.; Ding, Y.; Wang, Z. L. Synthesis of Tetrahexahedral Platinum Nanocrystals with High-Index Facets and High Electro-Oxidation Activity. *Science* **2007**, *316*, 732−735.
(31) Tian, N.; Zhou, Z. Y.; Sun, S. G.; Cui, L.; Ren, B.; Tian, Z. Q. Electrochemical Preparation of Platinum Nanothorn Assemblies with High Surface Enhanced Raman Scattering Activity. *Chem. Commun.* **2006**, 4090−4092.
(32) Zhang, D. F.; Diao, P.; Zhang, Q. Potential-Induced Shape Evolution of Gold Nanoparticles Prepared on ITO Substrate. *J. Phys. Chem. C* **2009**, *113*, 15796−15800.
(33) Tian, Y.; Liu, H.; Zhao, G.; Tatsuma, T. Shape-Controlled Electrodeposition of Gold Nanostructures. *J. Phys. Chem. B* **2006**, *110*, 23478−23481.
(34) Li, Y.; Diao, P.; Jin, T.; Sun, J.; Xu, D. Shape-Controlled Electrodeposition of Standing Rh Nanoplates on Indium Tin Oxide Substrates and Their Electrocatalytic Activity Toward Formic Acid Oxidation. *Electrochim. Acta* **2012**, *83*, 146−154.
(35) Gu, C.; Zhang, T.-Y. Electrochemical Synthesis of Silver Polyhedrons and Dendritic Films with Superhydrophobic Surfaces. *Langmuir* **2008**, *24*, 12010−12016.
(36) Tian, N.; Zhou, Z. Y.; Yu, N. F.; Wang, L. Y.; Sun, S. G. Direct Electrodeposition of Tetrahexahedral Pd Nanocrystals with High-Index Facets and High Catalytic Activity for Ethanol Electrooxidation. *J. Am. Chem. Soc.* **2010**, *132*, 7580−7581.
(37) Jia, F. L.; Wong, K. W.; Zhang, L. Z. Electrochemical Synthesis of Nanostructured Palladium of Different Morphology Directly on Gold Substrate through a Cyclic Deposition/Dissolution Route. *J. Phys. Chem. C* **2009**, *113*, 7200−7206.
(38) Fang, Y. X.; Guo, S. J.; Zhu, C. Z.; Dong, S. J.; Wang, E. K. Twenty Second Synthesis of Pd Nanourchins with High Electrochemical Activity through an Electrochemical Route. *Langmuir* **2010**, *26*, 17816−17820.
(39) Song, Y. J.; Kim, J. Y.; Park, K. W. Synthesis of Pd Dendritic Nanowires by Electrochemical Deposition. *Cryst. Growth Des.* **2009**, *9*, 505−507.
(40) McLellan, J. M.; Li, Z. Y.; Siekkinen, A. R.; Xia, Y. N. The SERS Activity of a Supported Ag Nanocube Strongly Depends on Its Orientation Relative to Laser Polarization. *Nano Lett.* **2007**, *7*, 1013−1017.
(41) Chen, H. J.; Wei, G.; Ispas, A.; Hickey, S. G.; Eychmüller, A. Synthesis of Palladium Nanoparticles and Their Applications for Surface-Enhanced Raman Scattering and Electrocatalysis. *J. Phys. Chem. C* **2010**, *114*, 21976−21981.
(42) Pan, W.; Zhang, X.; Ma, H.; Zhang, J. Electrochemical Synthesis, Voltammetric Behavior, and Electrocatalytic Activity of Pd Nanoparticles. *J. Phys. Chem. C* **2008**, *112*, 2456−2461.
(43) Wiley, B. J.; Xiong, Y. J.; Li, Z. Y.; Yin, Y. D.; Xia, Y. N. Right Bipyramids of Silver: A New Shape Derived from Single Twinned Seeds. *Nano Lett.* **2006**, *6*, 765−768.
(44) Xiong, Y. J.; McLellan, J. M.; Yin, Y. D.; Xia, Y. N. Synthesis of Palladium Icosahedra with Twinned Structure by Blocking Oxidative Etching with Citric Acid or Citrate Ions. *Angew. Chem., Int. Ed.* **2007**, *46*, 790−794.
(45) Abdelmoti, L. G.; Zamborini, F. P. Potential-Controlled Electrochemical Seed-Mediated Growth of Gold Nanorods Directly on Electrode Surfaces. *Langmuir* **2010**, *26*, 13511−13521.
(46) Xia, Y. N.; Xiong, Y. J.; Lim, B.; Skrabalak, S. E. Shape-Controlled Synthesis of Metal Nanocrystals: Simple Chemistry Meets Complex Physics? *Angew. Chem., Int. Ed.* **2009**, *48*, 60−103.
(47) Xiong, Y. J.; Xia, Y. N. Shape-Controlled Synthesis of Metal Nanostructures: The Case of Palladium. *Adv. Mater.* **2007**, *19*, 3385−3391.
(48) Huang, Y. F.; Zhu, H. P.; Liu, G. K.; Wu, D. Y.; Ren, B.; Tian, Z. Q. When the Signal Is Not from the Original Molecule To Be Detected: Chemical Transformation of para-Aminothiophenol on Ag during the SERS Measurement. *J. Am. Chem. Soc.* **2010**, *132*, 9244−9246.
(49) Osawa, M.; Matsuda, N.; Yoshii, K.; Uchida, I. Charge Transfer Resonance Raman Process in Surface-Enhanced Raman Scattering from p-Aminothiophenol Adsorbed on Silver: Herzberg-Teller Contribution. *J. Phys. Chem.* **1994**, *98*, 12702−12707.
(50) Kim, K.; Kim, K. L.; Shin, K. S. Visible-Light Response of 4-Aminobenzenethiol and 4,4′-Dimercaptoazobenzene Silver Salts. *J. Phys. Chem. C* **2013**, *117*, 5975−5981.
(51) Wang, L. M.; Wang, L. H.; Tan, E. Z.; Guo, L.; Han, X. D. Shaping Surface of Palladium Nanospheres Through the Control of Reaction Parameters. *Nanotechnology* **2011**, *22*, 305712−305717.
(52) Zhou, Q.; Fan, Q.; Zhuang, Y.; Li, Y.; Zhao, G.; Zheng, J. Effect of Substrate on Surface-Enhanced Raman Scattering of Molecules Adsorbed on Immobilized Silver Nanoparticles. *J. Phys. Chem. B* **2006**, *110*, 12029−12033.
(53) Zhang, D. F.; Niu, L. Y.; Jiang, L.; Yin, P. G.; Sun, L. D.; Zhang, H.; Zhang, R.; Guo, L.; Yan, C. H. Branched Gold Nanochains Facilitated by Polyvinylpyrrolidone and Their SERS Effects on p-Aminothiophenol. *J. Phys. Chem. C* **2008**, *112*, 16011−16016.
(54) Wang, Z. L. Transmission Electron Microscopy of Shape-Controlled Nanocrystals and Their Assemblies. *J. Phys. Chem. B* **2000**, *104*, 1153−1175.

(55) Zhang, J.-M.; Ma, F.; Xu, K.-W. Calculation of The Surface Energy of FCC Metals with Modified Embedded-Atom Method. *Appl. Surf. Sci.* **2004**, *229*, 34−42.
(56) Berhault, G.; Bausach, M.; Bisson, L.; Becerra, L.; Thomazeau, C.; Uzio, D. Seed-Mediated Synthesis of Pd Nanocrystals: Factors Influencing a Kinetic- or Thermodynamic-Controlled Growth Regime. *J. Phys. Chem. C* **2007**, *111*, 5915−5925.
(57) Xiong, Y.; Xia, Y. Shape-Controlled Synthesis of Metal Nanostructures: The Case of Palladium. *Adv. Mater.* **2007**, *19*, 3385−3391.
(58) Srivastava, S. C.; Newman, L. Mixed Ligand Complexes of Palladium(II) with Chloride and Bromide. *Inorg. Chem.* **1966**, *5*, 1506−1510.
(59) Feldberg, S.; Klotz, P.; Newman, L. Computer Evaluation of Equilibrium Constants from Spectrophotometric Data. *Inorg. Chem.* **1972**, *11*, 2860−2865.
(60) Jin, M.; Zhang, H.; Xie, Z.; Xia, Y. Palladium Concave Nanocubes with High-Index Facets and Their Enhanced Catalytic Properties. *Angew. Chem., Int. Ed.* **2011**, *50*, 7850−7854.
(61) Xiong, Y.; Cai, H.; Yin, Y.; Xia, Y. Synthesis and Characterization of Fivefold Twinned Nanorods and Right Bipyramids of Palladium. *Chem. Phys. Lett.* **2007**, *440*, 273−278.
(62) Nichols, R. J.; Burgess, I.; Young, K. L.; Zamlynny, V.; Lipkowski, J. A Quantitative Evaluation of the Adsorption of Citrate on Au(111) Using SNIFTIRS. *J. Electroanal. Chem.* **2004**, *563*, 33−39.
(63) Kunze, J.; Burgess, I.; Nichols, R.; Buess-Herman, C.; Lipkowski, J. Electrochemical Evaluation of Citrate Adsorption on Au(111) and the Stability of Citrate-Reduced Gold Colloids. *J. Electroanal. Chem.* **2007**, *599*, 147−159.
(64) Grden, M.; Lukaszewski, M.; Jerkiewicz, G.; Czerwinski, A. Electrochemical Behaviour of Palladium Electrode: Oxidation, Electrodissolution and Ionic Adsorption. *Electrochim. Acta* **2008**, *53*, 7583−7598.
(65) Diao, P.; Guo, M.; Zhang, Q. How Does the Particle Density Affect the Electrochemical Behavior of Gold Nanoparticle Assembly? *J. Phys. Chem. C* **2008**, *112*, 7036−7046.
(66) Cao, L. Y.; Diao, P.; Tong, L. M.; Zhu, T.; Liu, Z. F. Surface-Enhanced Raman Scattering of p-Aminothiophenol on a Au(core)/Cu(shell) Nanoparticle Assembly. *ChemPhysChem* **2005**, *6*, 913−918.
(67) Ruan, F. X.; Zhang, S. P.; Li, Z. P.; Yang, Z. L.; Wu, D. Y.; Ren, B.; Xu, H. X. Near-Field Coupling and SERS Effects of Palladium Nanoparticle Dimers. *Chin. Sci. Bull.* **2010**, *55*, 2930−2936.
(68) Liu, Z.; Yang, Z. L.; Cui, L.; Ren, B.; Tian, Z. Q. Electrochemically Roughened Palladium Electrodes for Surface-Enhanced Raman Spectroscopy: Methodology, Mechanism, and Application. *J. Phys. Chem. C* **2007**, *111*, 1770−1775.
(69) Gersten, J.; Nitzan, A. Electromagnetic Theory of Enhanced Raman Scattering by Molecules Adsorbed on Rough Surfaces. *J. Chem. Phys.* **1980**, *73*, 3023−3037.
(70) Liao, P. F. Lightning Rod Effect in Surface Enhanced Raman Scattering. *J. Chem. Phys.* **1982**, *76*, 751−752.